Thin-Film Morphology Control in Naphthalene-Diimide-Based Semiconductors: High Mobility n-Type Semiconductor for Organic Thin-Film Transistors

Deepak Shukla,* Shelby F. Nelson, Diane C. Freeman, Manju Rajeswaran, Wendy G. Ahearn, Dianne M. Meyer, and Jeffrey T. Carey

Kodak Research Laboratories, Eastman Kodak Company, Rochester, New York 14650

Received July 29, 2008. Revised Manuscript Received October 27, 2008

In organic thin film transistors (OTFT), the morphology and microstructure of an organic thin film has a strong impact on the charge carrier mobility and device characteristics. To have well-defined and predictable thin film morphology, it is necessary to adapt the basic structure of semiconducting molecules in a way that results in an optimum crystalline packing motif. Here we introduce a new molecular design feature for organic semiconductors that provides the optimized crystalline packing and thin film morphology that is essential for efficient charge-carrier transport. Thus, cyclohexyl end groups in naphthalene diimide assist in directing intermolecular stacking leading to a dramatic improvement in field effect mobility. Accordingly, OTFT devices prepared with vapor deposited *N*,*N*′-bis(cyclohexyl) naphthalene-1,4,5,8-bis(dicarboximide) (**1**) regularly exhibit field effect mobility near 6 $cm^2/(V\ s)$, which is one of the highest carrier mobilities reported for either n- or p-type organic semiconducting thin films.

Introduction

Over the past two decades, interest in organic thin film transistors (OTFTs) and their use in various technological applications has grown significantly.[1] Although a number of organic semiconductor materials have been developed for OTFT applications, most of the materials exhibiting high charge carrier mobility and device performance are p-type.[2,3] Comparatively, only a limited number of n-type organic semiconducting materials have been developed, and their performance to date remains far inferior to the best p-type materials.[2,3] Because of the lack of clear "structure−property" relationships for organic semiconductor design, the development of stable, high performing n-type materials continues to be a major challenge. It is widely recognized that the morphology and microstructure of an organic thin film has a strong impact on the charge carrier mobility and OTFT device characteristics. In general, organic materials that form highly oriented polycrystalline thin films exhibit high charge carrier mobility.[4] At the molecular level, it is the basic chemical structure of the molecule that controls intermolecular interactions that determines if a material will be crystalline or amorphous. Thus, to have well-defined thin film morphology it is necessary to control materials on the molecular scale. This necessitates adapting the basic structure of semiconducting molecules in a way that results in an optimum crystalline packing motif. Here we show that in *N*,*N*′-disubstituted naphthalene diimides (NDI)-based semiconductors, the cyclohexyl group provides a simple and effective way to control the crystalline packing motif and overall thin film morphology, resulting in one of the highest observed carrier mobilities in n-type OTFTs based on this material.

Among n-type semiconductors, naphthalene diimide (NDI) and perylene diimide (PDI)-based systems have been studied extensively.[5−8] An attractive characteristic of these systems is that the π-orbital wave functions form nodes at the two nitrogen positions in the diimide rings.[6] This feature allows for easy variation of substituents on nitrogens without affecting the electronic structure significantly. It has been shown that in *n*-alkyl substituted PDI based n-type OTFTs, thin film morphologies, electronic coupling between neighboring molecules, and carrier mobilities are very sensitive to the length of n-alkyl chains. Crystallographic data,[9,10] and theoretical calculations[3] attribute this to subtle changes in molecular packing motif that results in better π-orbital overlap between neighboring molecules. However, such a dramatic effect of n-alkyl chains on carrier mobility is not

* Corresponding author. E-mail: Deepak.Shukla@kodak.com.

(1) Klauk, H. *Organic Electronics: Materials, Manufacturing, and Applications*; Wiley-VCH Verlag GmbH & Co. KgaA: Wiinheim, Germany, 2006.
(2) Facchetti, A. *Materials Today* **2007**, *10*, 28, and references cited therein.
(3) Newman, C. R.; Frisbie, C. D.; da Silva Filho, D. A.; Brédas, J. L.; Ewbank, P. C.; Mann, K. R. *Chem. Mater.* **2004**, *16*, 4436.
(4) Dimitrakopoulos, C. D.; Malenfant, P. R. L. *Adv. Mater.* **2002**, *14*, 99.
(5) Katz, H. E.; Johnson, J.; Lovinger, A. J.; Li, W. *J. Am. Chem. Soc.* **2000**, *122*, 7787.
(6) Katz, H. E.; Lovinger, A. J.; Johnson, J.; Kloc, C.; Siegrist, T.; Li, W.; Lin, Y.-Y.; Dodabalapur, A. *Nature* **2000**, *404*, 478.
(7) (a) Chesterfield, R. J.; McKeen, J. C.; Newman, C. R.; Ewbank, P. C.; da Silva Filho, D. A.; Brédas, J. L.; Miller, L. L.; Mann, K. R.; Frisbie, C. D. *J. Phys. Chem. B* **2004**, *108*, 1928. (b) Chesterfield, R. J.; McKeen, J. C.; Newman, C. R.; Frisbie, C. D.; Ewbank, P. C.; Mann, K. R.; Miller, L. L. *Appl. Phys. Lett.* **2004**, *95*, 6396. (c) Jones, B. A.; Ahrens, M. J.; Yoon, M.620; Facchetti, A.; Marks, T. J.; Wasielewski, M. R. *Angew. Chem., Int. Ed.* **2004**, *43*, 6363.
(8) Kazmaier, P. M.; Hoffmann, R. *J. Am. Chem. Soc.* **1994**, *116*, 9684.
(9) Haedicke, E.; Graser, F. *Acta Crystallogr., Sect. C* **1986**, *C42*, 189.
(10) Klebe, G.; Graser, F.; Hadicke, E.; Bernot, J. *Acta Crystallogr., Sect. B* **1989**, *45*, 69.

10.1021/cm802071w CCC: $40.75
Published on Web 12/02/2008

entirely predictable. For instance, NDIs, which have a similar electronic structure, do not exhibit a similar sensitivity to n-alkyl chain substitution.[5,6] We speculated that conformationally rigid cycloalkyl substituents would change the crystalline packing in NDIs, and perhaps improve it relative to linear n-alkyl chains. From a variety of available cycloakyl groups we selected cyclohexane as the substituent to probe this hypothesis. The choice of cyclohexane was dictated by its uniqueness among cycloalkanes. Cyclohexane exhibits greater conformational rigidity and exists almost exclusively in a chair form, in which angular strain, torsional strain and nonbonded interactions are minimized. Furthermore, because bulky substituents in cyclohexane tend to adopt equatorial positions, it should further increase the conformational rigidity of the overall molecule. Cyclohexyl as an end group has been previously used to affect crystalline packing, and thin film morphology, in oligothiophene, oligothiophene-fluorene, and perylene diimide based organic semiconductors.[7c,11] However, because of the large size of the inner core in these systems cyclohexyl end groups had little influence on overall crystalline packing arrangement and carrier mobility.

Experimental Section

General. Chemicals were purchased from Aldrich and used as received. ^{1}H NMR (500 MHz) and ^{13}C NMR (500 MHz) spectra were obtained on a Varian Inova narrow-bore multinuclear NMR Spectrometer using tetramethylsilane as internal standard. Because of their limited solubility, ^{1}H and ^{13}C NMR spectra of **1** and **2** were recorded at 120 °C in CD_2Cl_2 solvent. MS spectra (MALDI-MS) were obtained on TofSpec2E Laser TOF mass spectrometer (Micromass, Inc., U.K.).

General Synthetic Procedure. The diimides **1** and **2** were prepared, following reported procedure,[12] by direct condensation of naphthalene dianhydride with the appropriate amine. Accordingly, a mixture of 1,4,5,8-naphthalenetetracarboxylic acid anhydride (1.34 g, 5.00 mmol), cyclohexylamine or n-hexylamine (30 mmol), and zinc acetate (50 mg) in 15 mL quinoline was heated at 140−150 °C for four hours. The mixture was cooled and diluted with several volumes of methanol. The resulting slurry was filtered; the collected solid washed with methanol and dried in air. The crude product was then purified by train sublimation at 1×10^{-4} to 1×10^{-6} torr.

***N,N′*-Bis(cyclohexyl) Naphthalene-1,4,5,8-bis(dicarboximide) (*1*).** ^{1}H NMR (CD_2Cl_2, 500.05 MHz): δ 8.76 (s, 4H), 5.10 (t, 2H, $J = 12$ Hz), 2.64 (dt, 2H, $J = 12$ and 11.7 Hzs), 1.57 (dt, 2H, $J = 12$ and 11.7 Hz), 2.03 (d, 2H, $J = 12$ Hz), 1.87 (d, 2H, $J = 12$ Hz), 1.47 (m, 2H). ^{13}C (CD_2Cl_2, 500.05 MHz): *d* 163.23, 130.74, 127.13, 126.70, 54.85, 29.38, 26.66, 25.52. MS (MALDI-TOF) *m/z* calcd for [$C_{26}H_{26}N_2O_4$], 430.5; found, 430.2.

***N,N′*-Bis(hexyl)-Naphthalene-1,4,5,8-bis(dicarboximide) (*2*).** ^{1}H NMR (CD_2Cl_2, 500.05 MHz): $\delta = 8.71$ (s, 4H), 4.16 (t, 4H, $J = 7.8$ Hz), 1.72 (m, 4H), 1.42 (m, 4H), 1.35 (m, 8H), 0.90 (t, 6H, $J = 7.2$ Hz). ^{13}C (CD_2Cl_2, 500.05 MHz): *d* 163.1, 130.99, 126.98, 41.15, 31.08, 28.2, 27.1, 22.93, 14.17. MS (MALDI-TOF) *m/z* calcd for [$C_{26}H_{30}N_2O_4$], 434.5; found, 434.2.

Preparation of Octadecyltricholrosilane (OTS)-Modified SiO_2/Si Wafer. Si/SiO_2 wafers were cleaned by immersion in a piranha solution (a mixture of 7:3 (v/v) of 98% H_2SO_4 and 30% H_2O_2). **Caution**: *Piranha solution reacts violently with organic compounds and should not be stored in closed containers for 30 min.* The wafers were then removed from the piranha solution and rinsed five to six times with copious amounts of deionized water. Wafers were blown dry with nitrogen and used immediately.

Clean wafers were then immersed in an unstirred solution of octadecyltricholrosilane ($\sim 2.6 \times 10^{-4}$ M) in anhydrous heptane and kept in a chamber maintained at constant 50% humidity for a period of 24 h. At the end of the immersion time, wafer was removed from the silanizing solution and immersed in anhydrous heptane and sonicated for about 30 min. Wafers were then rinsed with deionized water followed by anhydrous ethanol and 50% isopropanol-water (v/v) mixture. The thickness of the monolayer (ca. 30 Å) was determined by ellipsometery (J. A. Woollam, Alpha-SE ellipsometer) and was found comparable to the reported value.[13]

Thin-Film Characterization. The X-ray diffraction (XRD) data were collected in the reflection mode geometry using a Bragg−Brentano diffractometer equipped with a copper rotating anode, diffracted beam graphite monochromator tuned to Cu Kα radiation, and a scintillation detector. Data were collected in continuous mode at a scanning rate of 2° 2θ/min. Powder patterns of **1** and **2** were also taken on the same system.

Single-crystal diffraction data were collected at room temperature using Nonius KappaCCD diffractometer with graphite monochromated Mo Kα radiation ($\lambda = 0.71073$Å) using fine-focus sealed tube. Diffraction frames were collected using $\phi + \omega$ scans to fill the asymmetric unit. The first 10 frames were used for indexing reflections using DENZO package and refined to obtain final cell parameters. Data reductions were performed using DENZO-SMN. The structures were solved by using the direct methods, SIR97 and refined by full-matrix least-squares on F^2 with anisotropic displacement parameters for the non-hydrogen atoms using SHELXTL. The hydrogen atoms were incorporated into idealized positions. Material Studio software by Accelrys was used to generate structural diagrams. Crystallographic data (excluding structure factors) for the structure(s) reported in this paper have been deposited with the Cambridge Crystallographic Data Centre as supplementary publication nos. CCDC-671518 and 671519. Copies of the data can be obtained free of charge from www.ccdc.cam.ac.uk/conts/retrieving.html.

Film grain structure and morphology were examined by atomic force microscopy (AFM) using a NanoscopeR Dimension 3100 scanning probe microscope instrument in tapping mode. All experiments were carried out in an environmentally controlled laboratory (relative humidity set at 20%) using single crystal silicon Nanoprobes tips with a spring constant of ca. 17−43 N m^{-1} and resonance frequencies in the 262−359 kHz.

Thin-Film Transistor Device Preparation and Testing. Thin film transistors were made using the bottom-gate, top-contact geometry. The substrate used was a heavily doped silicon wafer, which also served as the gate of the transistor. The gate dielectric was a thermally grown SiO_2 layer with a thickness of 185 nm. For most of the experiments, the oxide surface was modified with self-assembled monolayer (SAM) of octadecyltrichlorosilane (OTS). Typically, an untreated oxide sample was included in the experiments for comparison.

The devices were made by vacuum deposition of **1** and **2** onto OTS modified SiO_2/Si substrates held at constant temperature by a resistively heated and water-cooled copper block. The base pressure in the evaporation system was 2 x10^{-7} Torr and stayed below 8 x10^{-7} Torr during the deposition. The deposition rate was 0.1 Å/s while the substrate temperature (T_{dep}) was held at 20 or 75 °C for

(11) Locklin, J.; Li, D.; Mannsfeld, S. C. B.; Borkent, E.-J.; Meng, H.; Advincula, R.; Bao, Z. *Chem. Mater.* **2005**, *17*, 3366.
(12) Rademacher, A.; Maerkle, S.; Langhals, H. *Chem. Ber.* **1982**, *115*, 2927.
(13) Tillman, N.; Ulman, A.; Schildkraut, J. S.; Penner, T. L. *J. Am. Chem. Soc.* **1988**, *110*, 6136.

most experiments. The thickness of the organic layer, measured by a calibrated quartz crystal monitor, was typically 17−25 nm. Source and drain electrodes were defined by thermal evaporation of 500 Å of gold through a shadow mask onto the semiconductor film. Puratronic (99.999%) grade gold was obtained from Alfa Aesar (Ward Hill, MA). The base pressure in the metal evaporation chamber was 5×10^{-6} Torr, and stayed below 8×10^{-6} Torr during deposition. The channel width was 650 μm, while the channel lengths were varied between 50 and 150 μm. The sample was exposed to the ambient between the organic semiconductor deposition and the source and drain gold contact deposition. Devices were isolated by a probe-tip scratch closely encircling the outer perimeter of contacts and channel.

Device Measurement and Analysis. Electrical characterization of the fabricated devices was performed with a Hewlett-Packard HP 4145b parameter analyzer. The probe measurement station was held in a positive argon or oxygen environment for all measurements with the exception of those purposely testing the stability of the devices in air. Electrical measurements at higher humidity levels were carried out by bubbling argon and/or oxygen through a bubbler containing water. The humidity level at the probe station was measured using a digital hygrometer (VWR, ± 4% accuracy). All device fabrication and electrical measurements were performed under sodium lighting. The devices were exposed to air prior to testing. For each experiment performed, between 4 and 12 individual devices were tested on each sample prepared, and the results were averaged. For each device, the source-drain current (I_{SD}) was measured as a function of source-drain voltage (V_{SD}) for various values of gate voltage (V_G). For most devices, V_{SD} was swept from 0 to 100 V for each of the gate voltages measured, typically 25, 50, 75, and 100. In these measurements, the gate current (I_g) was also recorded in order to detect any leakage current through the device. Furthermore, for each device the drain current was measured as a function of gate voltage for various values of source-drain voltage. For most devices, V_g was swept from 0 to 100 V for each of the drain voltages measured, typically 25, 50, 75, and 100 V.

Results and Discussion

The crystalline packing motif of cyclohexyl substituted *N*,*N*′-bis(cyclohexyl)naphthalene diimide (**1**), and its concomitant effects on thin film morphology and carrier mobility in OTFT devices, was compared with a linear n-hexyl chain containing analogue, *N*,*N*′-bis(hexyl)naphthalene diimide (**2**).

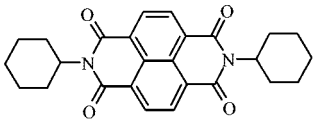

1

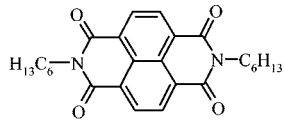

2

The single crystals of **1** were grown by train sublimation, whereas good quality crystals of **2** could only be obtained from solution by slow diffusion of hexane into a chloroform solution of **2**. However, the crystals of **2** were not of good quality (twinned and weakly diffracting), which affected data quality.

Figure 1a shows the single crystal structure of *N*,*N*′-bis(cyclohexyl)naphthalene diimide (**1**), wherein cyclohexane rings are in the chair conformation with naphtahlene diimide at equatorial positions. Figure 1b shows the long-range crystalline packing motif of **1** in the solid state. For the sake of clarity the cyclohexane rings have been omitted in the

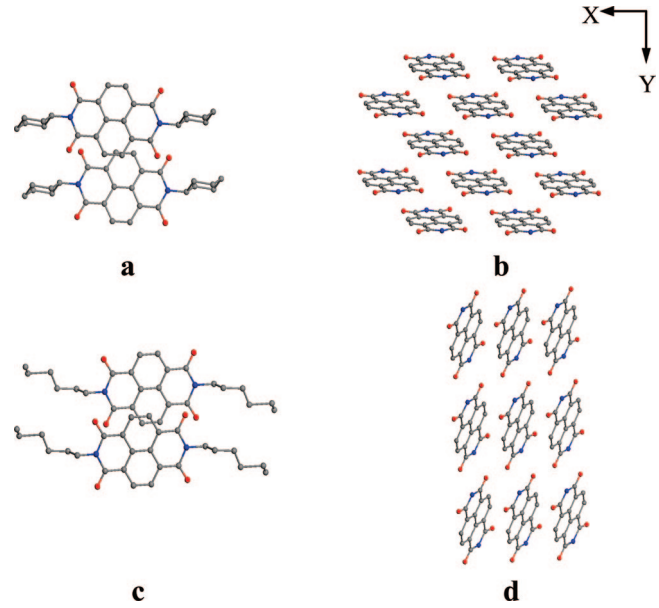

Figure 1. Crystal structure and solid state packing of **1** and **2**. (a) The molecular structure of **1**. (b) Crystalline packing motif of **1** (cyclohexane rings omitted for clarity). (c) The molecular structure of **2**. (d) Crystalline packing motif of **2** (*n*-hexane chain omitted for clarity).

Figure 1b. It is evident from Figure 1b that along the stacking direction, the naphthalene diimide cores are not cofacial and are displaced along both the short and the long axes of the molecule, the largest displacement being along the short axis of the molecule. In this packing motif, the closest distance between the two closest molecules of **1** is approximately 3.34 Å along the *y*-axis (Figure 1b).

In contrast, in the crystal structure of *N*,*N*′-bis(*n*-hexyl) naphthalene diimide (**2**), the *n*-hexyl group adopts a nonextended conformation, with only a part of the alkyl chain in all-trans conformation (Figure 1c). It is not clear why the *n*-hexyl chain does not adopt an energetically favorable all-trans conformation. In the solid state, **2** also exhibits long-range stacking; however, because of unfavorable steric interactions and larger volume fraction demand of *n*-hexyls, the naphthalene diimide cores are not only displaced along the short axis but also along the long axis (Figure 1d). The nearest distance between two neighboring molecules along *x*- and *y*-axes is ∼ 4.9 and 8.3 Å, respectively.

The differences in crystalline packing of **1** and **2** have a dramatic impact on their respective carrier mobilities in OTFT devices. To probe carrier transport properties, bottom-gate n-type OTFT device incorporating **1** and **2** were made by evaporating thin films (175−200 Å at a rate of 0.1 Å/ s) on octadecyltrichlorosilane (OTS)-modified SiO_2/Si and SiO_2/Si substrate held at temperatures (T_{dep}) of 25 °C. The devices were fabricated in "top contact" geometry, where the heavily doped silicon substrate served as the gate electrode, and gold (Au) source and drain electrodes (50 nm thick, 200 μm × 650 μm wide) were thermally evaporated through a shadow mask on the organic semiconductor layer. The OTFT devices had a variable channel length (L) of 50, 100, and 150 μm, a constant width (W) of 650 μm, and a SiO_2 gate dielectric thickness of 185 nm. The electrical performance was measured under a continuous stream of

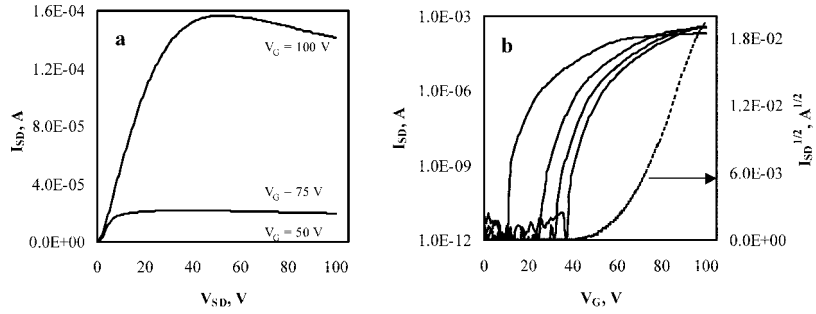

Figure 2. $I-V$ characteristics of exemplary OTFT devices based on **1** coated on OTS-treated SiO_2/Si substrate with 150 μm channel length and 650 μm channel width: (a) output curves at gate voltages V_G = 50, 75, and 100 V. (b) Transfer characteristics for the same device at V_{DS} = 25, 50, 75, and 100 V.

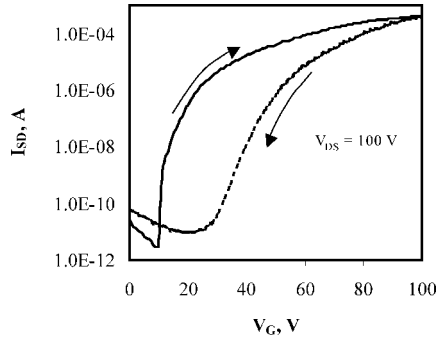

Figure 3. Hysteresis in the $I-V$ characteristics of an exemplary OTFT device based on **1** coated on OTS- modified SiO_2/Si substrate with 150 μm channel length and 650 μm channel width.

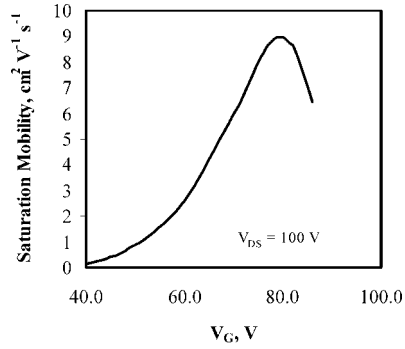

Figure 4. Field-effect saturation mobility (at V_{DS} = 100 V) of typical OTFT of **1** on OTS-modified SiO_2/Si wafer as a function of gate voltage.

argon or oxygen. The saturation field effect mobility, μ_{sat}, was extracted from a straight-line fit to the linear portion of the $\sqrt{I_D}$ versus V_G curve. (Figure 2b) in the saturation regime according to eq 1,

$$I_D = \frac{W}{2L}\mu_{sat}C_{ox}(V_G - V_{th})^2 \quad (1)$$

where L is the channel length, W is the channel width, C_{ox} is the capacitance of the SiO_2 insulating layer, V_G is the gate voltage, and V_{th} is the threshold voltage.

Typical characteristics of the n-type OTFTs based on **1** as semiconductor are shown in Figure 2. The electrical performance of **1** measured under a continuous stream of argon at 22% relative humidity showed n-type field effect operation. A saturation regime electron mobility of 6.2 cm^2 V^{-1} s^{-1} and current on/off ratio of 6×10^8 was extracted for V_{ds} = 100 V. Three sweeps at V_{ds} = 25 V, 50 V and 100 V are shown in Figure 2b, where the turn-on voltage in the first sweep is 10 V, whereas the subsequent sweeps see the turn-on voltage migrating to higher values and eventually pinning at the high value of 38V. A double I_D-V_G sweep at the constant V_{DS} shows hysteresis of the similar magnitude (Figure 3). This behavior is typical of **1** on OTS-modified SiO_2 substrate, as measured in dry argon, and subsequent sweeps show little or no further migration. We ascribe this behavior to presence of O_2 and H_2O at the semiconductor-dielectric interface (vide infra).

During repeated runs (approximately 200 runs), typical saturation mobility values peak in the range from 4.5 to 6.5 cm^2 V^{-1} s^{-1}. Saturation mobility up to 7.5 cm^2 V^{-1} s^{-1} were obtained when devices were tested after prolonged equilibration (ca. 30 min.) in an argon atmosphere at low humidity. This is one of the highest reported ranges of electron mobility[14] for an organic semiconductor in a thin film. However, as is the case with other organic thin-film transistors, the mobility of **1** is gate voltage dependent (Figure 4). The gate voltage dependence of mobility is usually indicative of the presence of defects and grain boundaries in the polycrystalline thin film.[15a,b] Figure 4 shows that the saturation mobility steadily increases with gate voltage and then decreases for gate biases in excess of around 85 V. At higher gate voltage, as more charges are injected into the conductive channel, the more these charges accumulate at the dielectric-semiconductor interface. The decrease in the mobility at high gate voltages in polycrystalline thin films is usually attributed to higher density of defects, which are detrimental to charge transport, at the insulator-semiconductor interface than in the remainder of the film.[15d,e]

These devices have high contact resistance, as is seen in the initial curvature of the I_D-V_D curve in Figure 2a. As a consequence, linear mobility is typically lower than saturation mobility, peaking at values of 1.8 cm^2 V^{-1} s^{-1} at V_D = 10 V. The effect of contact resistance is also evident in decreased saturation mobility with decreasing channel length. As the channel length is decreased from 150 to 50 μm, the relative

(14) Singh, Th. B.; Yang, H.; Plochberger, B.; Yang, L.; Sitter, L. H.; Neugebauer, H.; Sariciftci, N. S. *Phys. Status. Solidi* **2007**, *244*, 3845.
(15) (a) Necliudov, P. V.; Shur, M. S.; Gundlach, D. J.; Jackson, T. N. *J. Appl. Phys.* **2000**, 6594. (b) Horowitz, G.; Hajlaoui, M. E.; Hajlaoui, R. *J. Appl. Phys.* **2000**, *87*, 4456. (c) Klauk, H.; Schmid, G.; Radlik, W.; Weber, W.; Zhou, L.; Sheraw, C. D.; Nichols, J. A.; Jackson, T. N. *Solid-State Electron.* **2003**, *47*, 297–301. (d) Schon, J. H.; Batlogg, B. *J. Appl. Phys.* **2001**, *89*, 336. (e) Horowitz, G.; Lang, P.; Kalb, W.; Mottaghi, M.; Roumyantseva, A.; Yassar, A. *IPAP CS-6* **2005**, *6*, 125–129, Proceedings of the International Symposium on Super-Functionality Organic Devices 2004.

Table 1. Electrical Performance of OTFT Devices Incorporating 1 under Different Test Conditions

	dielectric	humidity (%)	T_{dep}[a] (°C)	test atmosphere[b]	μ^{avg} (σ)[c,d] ($cm^2\ V^{-1}s^{-1}$)	I_{on}/I_{off}[e]	V_{th}[f] (V)
i	OTS/SiO_2	22	22	Ar	6.2 (1.15)[g]	6×10^8	58
ii	OTS/SiO_2	22	22	O_2	5.5 (0.57)[h]	6×10^8	72
iii	OTS/SiO_2	22	22	Air	0.41	4×10^5	71
iv	SiO_2	22	22	Ar	$\sim 1 \times 10^{-4}$	4×10^3	62
v	OTS/SiO_2	60	22	Ar	1.8	2×10^7	73
vi	OTS/SiO_2	60	22	O_2	0.30	4×10^6	73

[a] T_{dep}, substrate temperature during deposition of **1**. [b] Samples were equilibrated in test atmosphere for 30−45 min. [c] μ^{avg} field-effect mobility. [d] Standard deviation. [e] I_{on}/I_{off}, current on to off ratio. [f] V_{th}, threshold voltage. [g] Standard deviation, $n = 21$. [h] Standard deviation, $n = 5$.

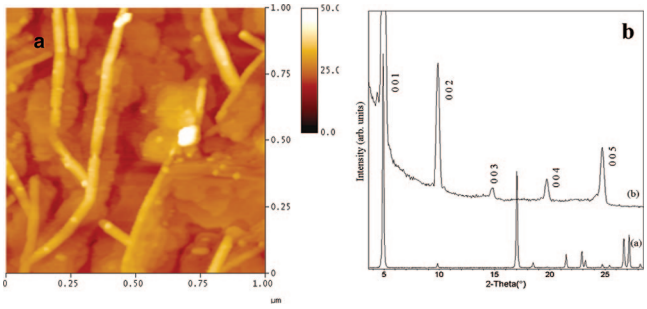

Figure 5. Vapor-deposited thin film (18 nm) of **1** on OTS-modified SiO_2/Si wafer: (a) 1 × 1 μm^2 AFM image of a thin film. (b) X-ray diffraction pattern of the same film (curve b) and powder pattern of **1** (curve a).

influence of the contact resistance is magnified compared to the relative influence of the channel resistance. Accordingly, for devices with W/L = 650/50 saturation mobility $\mu = 2.66$ (± 0.7) $cm^2\ V^{-1}\ s^{-1}$ was significantly lower than $\mu = 4.03$ (± 0.6) $cm^2\ V^{-1}\ s^{-1}$ for devices with $W/L = 650/100$.

In contrast, under similar device fabrication conditions, **2** gave a peak saturation mobility of only 0.16 $cm^2\ V^{-1}\ s^{-1}$. However, when OTFT devices of **2** were fabricated at higher deposition rate (ca. 10 Å/s) saturation mobilities up to 0.7 $cm^2\ V^{-1}\ s^{-1}$ were measured (see Figure 2S and Table 1S and in the Supporting Information for complete device data).

The field- effect mobility of **1** was independent of film growth rate over the range from 0.1 to 1.5 Å s^{-1} and exhibited dependence on the substrate temperature during deposition. Devices fabricated at higher deposition temperature ca. 75 °C gave lower mobility of 1.7 $cm^2\ V^{-1}\ s^{-1}$. At higher deposition temperature, films of **1** were significantly nonhomogeneous, probably because of significant differences in the thermal expansion coefficient for the organic film and the SiO_2 substrate, which results in organic film under tension upon cooling. The field-effect mobility was strongly dependent on experimental test conditions. The best field-effect mobility value of 6.2 $cm^2\ V^{-1}\ s^{-1}$ was obtained when **1** devices were tested at a low humidity level under a continuous stream of argon. Mobility of **1** was significantly lower when devices were operated in air or at higher humidity levels (entries iii, v, and vi, Table 1). The drop in mobility under these conditions is, as previously suggested, probably due to electron trapping by O_2 and/or H_2O at grain boundries.[5−7] Consistent with the previous observation that

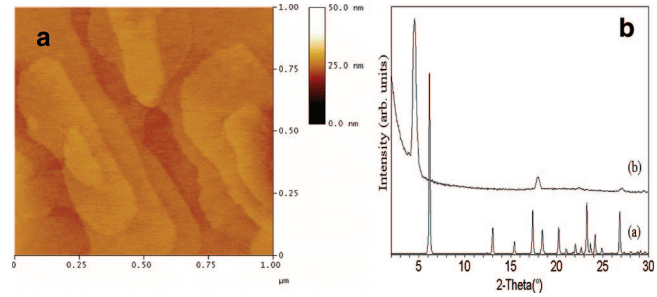

Figure 6. Vapor-deposited thin film (18 nm) of **2** on OTS-modified SiO_2/Si wafer: (a) 1 × 1 μm^2 AFM image of a thin film (b) X-ray diffraction pattern of the same film (curve b) and powder pattern of **2** (curve a).

hydroxylic functionalities act as electron traps at the dielectric-semiconductor interface,[16] mobility of **1** on untreated SiO_2/Si was particularly low (ca. 1×10^{-4}) (entry iv, Table 1).

The average V_{th} observed for the OTFT device of **1** is significantly higher than that observed in perfluorinated alkyl group containing NDI and PDI compound.[5,7c] This could possibly be due to denser packing of fluorocarbon tails, which acts as a barrier toward diffusion of O_2 and H_2O into the semiconductor film. It has been observed before that n-type OTFTs are particulary sensitive to O_2.[7a,b] In PDI-based OTFT devices, it has been demonstrated that oxygen at the semiconductor-dielectric interface acts like a trap leading to positive threshold voltage shift.[7a] Because all our devices were exposed to the ambient before testing, the presence of O_2 and/or H_2O at the semiconductor−dielectric interface could act as charge trap leading to the observed higher threshold voltage. This reasoning is supported when we compare redox properties of NDI and O_2 in hydroxylic vs nonhydroxylic solvents. On the basis of the redox data in acetonitrile, the reduction potential of NDI (ca. −0.65 V vs SCE) is similar to that for O_2 (ca. −0.65 V vs SCE)[17] and electron transfer from NDI radical anion to O_2 is isoenergetic and O_2 is a shallow trap for NDI radical anion. On the other hand, the reduction of O_2 in water is easier by ca. ∼ 0.5 V,[17] which makes electron transfer from NDI radical anion to O_2 energetically more favorable and O_2 acts as a much deeper electron trap. The observed higher V_{th} and lower mobility of devices tested under oxygen at higher humidity compared to those tested under Ar atmosphere and lower humidity (entries ii and vi, Table 1) is consistent with this proposed oxygen trapping mechanism.

The striking difference in carrier mobilities of **1** and **2** are better understood when we compare their thin film morphologies. The atomic force microscopic (AFM) image of a thin film of **1** shows layered densely packed polycrystalline film with an average feature size of 100−200 nm (Figure 5a). The X-ray diffractogram (XRD) of this film showed strong and narrow peaks up to the fifth order (Figure 5a), which is consistent with a crystalline film with preferred orientation of a family of molecular planes on the substrate interface. On the basis of the indexing from single-crystal data, the peak at $2\theta = 4.91°$ was assigned as the first-order reflection, (001), and the remaining peaks were successive

(16) Chua, L. L.; Zaumseil, J.; Chang, J.-F.; Ou, E. C.-W.; Ho, P. K.-H.; Sirringhaus, H.; Friend, R. H. *Nature* **2005**, *434*, 194.
(17) Sawyer, D. T.; Valentine, J. S. *Acc. Chem. Res.* **1981**, *14*, 393.

orders of reflections (Figure 5a). The match between single crystal peaks (curve a, Figure 5a) and the thin film peaks in XRD (curve b, Figure 5a) strongly suggests that the thin film has the same molecular packing motif as seen in the bulk crystal. It is important to note that this behavior is unlike that of many organic semiconductor films, which typically exhibit a thin-film phase that is distinct from the bulk crystal phase.[18] This bulk-crystallizing feature provides the desired structure−property predictability needed for organic semiconductor design. A significant consequence of this thin-film/bulk- phase similarity is that the film structure is less sensitive to, if not independent of, the material processing conditions, e.g., deposition rate, substrate temperature, and coating methodology. Furthermore, the close correspondence between the molecular length of **1** (17.5 Å, obtained from the crystal structure) and interlayer spacing of $d_{001} = 17.9$ Å in XRD suggests that thin films of **1** grow with the long axis of the molecule oriented out of the substrate plane. In this packing motif, thin film resembles the (001) layers in the bulk crystal of **1**, wherein the molecules are near vertical on the device plane leading to maximum electronic coupling between neighboring molecules.

In contrast, the AFM image of the thin film of **2** shows a polycrystalline film with significantly larger grain size (0.5−1 μm) (Figure 6a). However, the XRD of the thin film of **2** shows only two diffraction peaks (Figure 6b), and positions of these peaks do not match with the peaks calculated from the single crystal structure, indicating the presence of a thin film phase. That is, besides a low degree of ordering, **2** exhibits a different molecular orientation in the thin film from that observed in the bulk crystal structure. Since OTFT devices of both **1** and **2** were fabricated under similar conditions, the large difference in the carrier mobilities can be ascribed to the differences in crystal packing and thin film morphology.

(18) Fritz, S. E.; Martin, S. M.; Frisbie, C. D.; Ward, M. D.; Toney, M. F. *J. Am. Chem. Soc.* **2004**, *126*, 4084.

Conclusions

In summary, we have demonstrated that cyclohexyl substituent in naphthalene diimide based semiconductors provides the optimized crystalline packing and thin film morphology that is essential for efficient charge carrier transport. A dramatic improvement in field effect mobility is demonstrated for n-type NDI materials that include cyclohexyl groups to strategically direct intermolecular stacking. OTFT devices prepared with vapor deposited **1** regularly exhibit field effect mobilities near 6 $cm^2\ V^{-1}s^{-1}$ which is one of the highest carrier mobilities reported to date for either n- or p-type organic semiconducting thin films. The stereochemical attributes of the cyclohexyl groups provide a propensity for **1** to assemble into thin-films with bulk phase crystalline packing. This bulk-crystallizing feature lends predictability to semiconductor design, and furthermore, can provide needed processing latitude for OTFT preparation.

Acknowledgment. We are grateful to Dr. Jerome Lenhard, Dr. David Levy and Dr. Thomas Welter of Eastman Kodak Company for fruitful discussions and helpful comments.

Supporting Information Available: Output and transfer characteristics (Figure 1S) of OTFT devices of **2** and device performance under various deposition conditions (Table 1S) are available. This material is available free of charge via the Internet at http://pubs.acs.org.

CM802071W